Study on the Assessment of Fatigue Durability of Corroded Steel Girder Ends Repaired with Carbon Fiber Reinforced Polymer

Rusandi Noor[1], Hiroshi Tamura*[1], Hiroshi Katsuchi[1], Wang Jiaqi[1]

Department of Civil Engineering, Institute of Urban Innovation, Yokohama National University, 79-8 Tokiwadai, Hodogaya-ku ,Yokohama 240-8501, Japan

*email: tamura-hiroshi-jg@ynu.ac.jp
email: katsuchi@ynu.ac.jp
email: wang-jiaqi-nf@ynu.ac.jp

Abstract

Bridge maintenance and repair have gained significant attention as their service life continues to extend. Numerous retrofit projects have been implemented to address the corrosion issues at steel plate girders' ends. This study focuses on evaluating the durability of the retrofitted part of the steel girder end by assessing its ability to sustain eccentric fatigue load and recognizing the possibilities of CFRP post-retrofitted damage. The novel specimen was designed to replicate corrosion on the inner side of exterior steel girder web ends and study the effect of retrofitting them with CFRP. In addition, a new bending fixture design based on the specimen design was proposed to reproduce the actual severe loading mode of a CFRP-retrofitted steel girder end. Polyurea putty (FU-Z) was used to identify the durability owing to its flexible characteristics under fatigue. The lifecycle-oriented experimental results showed that the specimens with CFRP-retrofitted steel girder ends survived for 3.5 million cycles under fatigue loading. However, specimens without polyurea putty exhibited damage characteristics, such as detachment and delamination. In addition, the shifted local stress detection of the edge joint represented the detachment of the retrofit material at 3 million cycles. The detachment occurred at the end of the corrosion web edge and delamination was observed in the cutoff section, which reduced the local bonding of 50% of the CFRP sheets. In addition, local damage resulted in durability resistance developed under elastic conditions.

keywords: *Carbon fiber reinforced polymer reinforcement, fatigue, durability, damage initiation, polyurea putty, detachment, delamination*

Acknowledgment

Financial support is provided by the Japanese Government (MONBUKAGAKUSHO: Ministry of Education, Culture, Sports, Science, and Technology – MEXT). The scholarship made this research possible, and it is greatly appreciated.

Manuscript Length: 7297 words

1. Introduction

Steel plate girder ends columns are critical elements in bridge structures as they are responsible for bearing and transmitting vertical and lateral loads. Their part is important for the overall stability of the bridge. Thus, external bridge columns can experience failure when subjected to eccentric axial compression, often due to structural damage such as local corrosion at the inner side of the part. However, carbon fiber reinforced polymer (CFRP) reinforcement is used to upgrade the load capacity of corroded column steel bridge members owing to its high elasticity, corrosion resistance, and lightweight characteristics. Also, when the retrofitted area is small, these countermeasures are often efficient (PWRI, 2010).

Consequently, the durability of CFRP-strengthened corroded steel girder ends should be confirmed when it was implemented on service loading. The CFRP is often peeled from the steel plate only below the yield point of the steel when implementing a conventional carbon fiber sheet without polyurea putty as an adhesive layer. This is one of the factors affecting the long-term strength of CFRP along with its durability. Subsequently, fatigue experiments of girder-end retrofitted parts for durability investigations are prioritized.

Based on this, fatigue damage initiation criteria are essential for determining the damage type, time (cycles), and location. The damage initiation phase of CFRP reinforcements under fatigue loading has not been intensively investigated. Instead, damage initiation has always been described in a more predictive manner; that is, without intense physical evidence. Therefore, identifying damage tolerance is a challenge. Damage initiation in durability characteristics owing to fatigue is a complex process that is required to be detected and visualized.

Many investigators (Shenoy et al., 2007; Colombi et al., 2012; Yu et al., 2015; Liu et al., 2009; Zhang et al., 2021) have adopted cyclic fatigue loading as the experimental method, which results in the rapid failure of CFRP-reinforced specimens. Wakabayashi et al., (2013) investigated the behavior of corroded steel girder ends with CFRP reinforcement. However, the locations of damage initiation (buckling mode) in the unrepaired and repaired specimens were almost identical. In this study, we have explored the damage mode behavior further because the influence of CFRP reinforcement is not sufficient to shift the location of stress concentration of the repaired target.

The eccentric load of a large vehicle group can cause out-of-plane conditions in steel bridge components. Practical evidence was provided by Ghahremani et al., (2015). They assessed CFRP-repaired welded joints of a bridge as a result of distortion-induced fatigue. Al-Salih et al. (2021) investigated distortion-induced fatigue in bridge web gaps. They developed a novel repair method by attaching a CFRP part to the bridge to reduce localized stress in the web gap region.

Magi et al., (2016) defined the CFRP damage initiation as the first nucleation in the off-axis of the layers. It was observed that the initiation corresponded to the actual separation of different materials. Thus, damage initiation is a critical condition that changes the rate of structural degradation for a given load. Marco et al., (2021) studied the relationship between the compressive strength properties of unidirectional CFRP and identified the strong effect of fiber alignment on damage initiation.

Furthermore, matrix-initiated damage was reported by Skinner et al., (2019) The initial damage to the resin, which was known as primary damage, included the transition stage of the fatigue phase at approximately 10%. The initial damage in the matrix began to merge, thus forming macrocracks in the damaged region. Ammar et al., (2021) observed typical damage initiation followed by a sudden stress drop. This occurred for several reasons, including the effect of a significant change in the boundary of the material. This investigation also revealed preexisting voids in the specimens under microscopic conditions.

Therefore, we have conducted a comprehensive numerical study to discover the severe elements of the CFRP part by varying the type of simple supported steel girder bridge structure with 40 m span length – 2 lanes as described in one of the previous studies (Noor & Tamura, 2022) using finite element analysis (Abaqus, 2018). In addition, adequate research was conducted to identify the characteristics of local stress and deformation mode at steel girder ends reinforced by CFRP.

The primary objective of this work is to experimentally evaluate the durability of carbon fiber reinforced polymer (CFRP) reinforcement at the steel girder end due to eccentricity-induced fatigue with novel specimen design approaches in discovering damage initiation. The simplification of corrosion geometry was also generated. This evaluation will be conducted by subjecting the specimens to a constant-amplitude load fluctuation (CALF) during the experimentation process. The new strategy was investigated experimentally using a CFRP retrofitted specimen of height 441 mm (1/6 actual size) in a simplified steel girder end model, in which the specimen was subjected to cyclic loading. In addition, the possibility of visually assessing fatigue damage can be demonstrated.

2. Specimen Design

- **Material Parameter**

Specimen preparation is classified into the following stages: cutting, welding, and piercing with steel-grade SM400. For a material made of steel with a plate thickness of less than 40 mm, it is guaranteed that the compressive cyclic load does not create local buckling. The allowable axial compressive stress of the structural specimens is designed under 140 N/mm^2 (JRA, 2012). In addition, we have ensured that the specimen design is mentioned as a detailed category D in the Specification for Highway Bridges, Japan Road Association.

- **Compact Specimen Design**

Noor & Tamura, 2022 have conducted a numerical simulation to assess the severe section in retrofitted girder ends. Thus, schematic **Figure 1a** is provided to help the understanding of the replication process as it relates to the specimen's position and location on the severe region of the steel girder end.

As shown in **Figure 1b**, it is designed that the specimen is supported at both ends using pin supports and that the loads act on it with eccentricity. This assumption is made when a specimen between the fixing points on the compression side contains a target section in which the stresses are controlled. The characteristics of the specimens are determined to replicate the out-of-plane deformation, which is unrestrained at the target part. The CFRP specifications (NERI, 2015; Pham et al., 2021) for the anchoring length and shift length are set to 100 and 25 mm, respectively (**Figure 1b**). In this case, the epoxy putty (FB-ES9) was molded into an arc-like shape with R = 50 mm at the joint between the bottom flange and the web. This type of anchoring is important for this implementation. Moreover, this study calculated the layers of CFRP designed 7 sheets to act as a recovery part against 3 mm local corrosion. The number of carbon fiber sheets required (n) is determined in the way that the steel converted thickness (t_{cf}) of the sheets becomes larger than that of the maximum section loss (t_{sl}). The degree of stresses after reinforcement (σ_2) calculated by the following conditions should be less than the allowable stress (σ_a).

The following NERI, 2015 **Formula 1** using the fiber weight and the density of the carbon fiber of the carbon sheets:

$$t_{cf} = \frac{1000 \times w}{\rho} \qquad (1)$$

Where, w = 300 g/m^2 and ρ = 2.1x10^6 g/m^3. The number of laminated carbon fiber sheets should be determined by (NERI, 2015) **Formula 2** below:

$$n_{CFRP} = \frac{t_d}{\left(t_{cf} \times \frac{E_{cf}}{E_s}\right)} \tag{2}$$

Where, t_d = section loss (mm), E_{cf} = CFRP elastic modulus (kN/m^2), E_s = steel elastic modulus (kN/m^2).

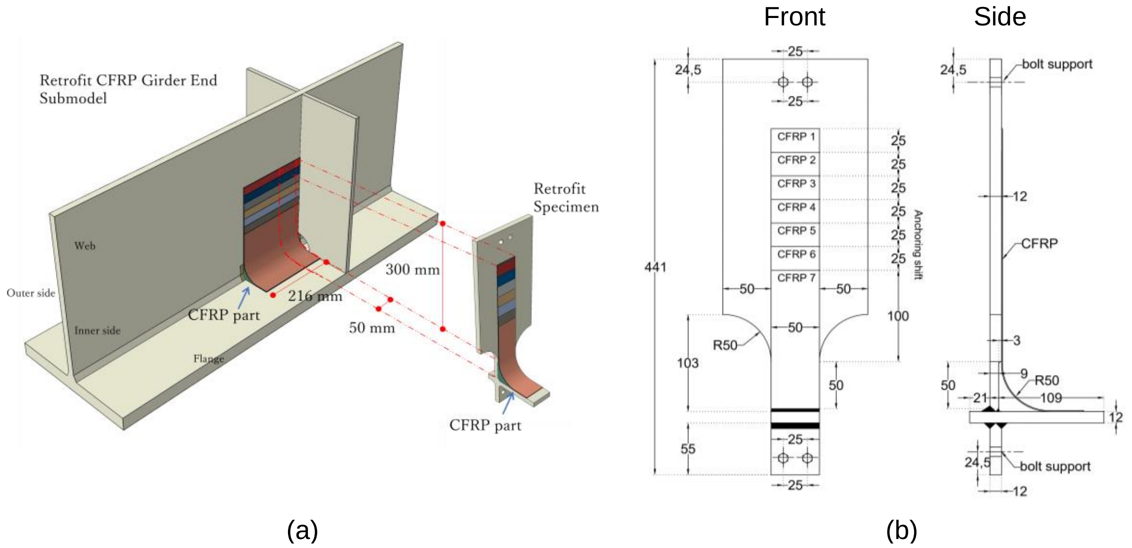

Figure 1 (a) Schematic of idealization of the compact specimen from steel girder end; (b) Compact specimen dimension (unit: mm)

However, in eccentric vehicle load situations, the live load will be off-center, thus causing out-of-plane compression in the column. When a steel girder end column is subjected to a load at the center, bending can be a severe problem and may be more important than the compression stress (Gil-Martín et al., 2010; Baumann & Hausmann et al., 2021; Graciano et al., 2014). In **Figure 2**, the new design of the cyclic loading parts is constructed from regular fixturing elements, such as grip plates, filler plates, bolt joints, and fixtures. The new part consists of the following elements:

1. Plate grip
   It was used to establish and maintain the position of the specimen in the fixture by constraining the movement of the part during compression.

2. Fixture
   The experimental setup adopted a proportional-type loading to create a compressive bending action. It was necessary to restrict the degrees of freedom while designing the setup. The reverse L-shaped design of the fixture is a new fixture model. This geometrical shape shown in **Figure 2(a-b)** can maintain the target condition such as the compressive load combined with out-of-plane deformation. Moreover, the movement may reach maximum displacement in elastic conditions.
3. Filler plate
   A filler comprising two plates was used to attach each specimen. The inner filler plate was designed to support out-of-plane bending deformation during cyclic loading.

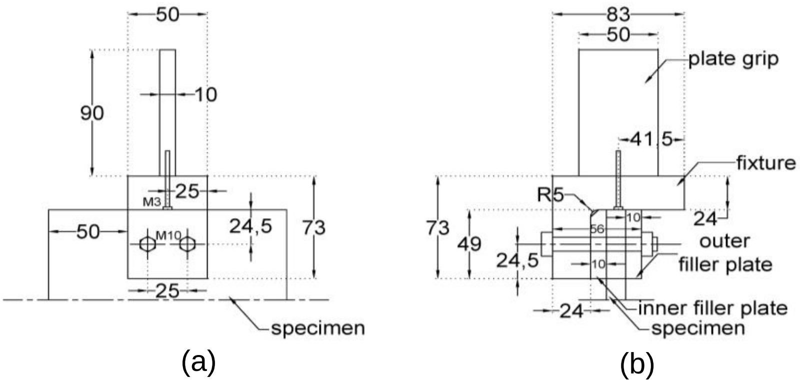

Figure 2 Fixture detail dimension: (a) Front view ;(b) Side view (unit: mm)

Figure 3a shows the arrangement and setup of the specimen before repairment in a cyclic machine. This setting placement is the key to producing the bending compressive cyclic load. As shown in **Figure 3b,** the detailed weld bead sizes and dimensions are adjusted from the web weld bead of the corroded girder end. The size of the specimen web weld bead is decreased by 1/5. The accuracy of the comparison of local stress distributions of the weld beads was considered in numerical simulation. As shown in **Figure 3b**, the depth of the surface loss and corroded web edge model has an optimum value of 3 mm to prevent local buckling. Also, the corrosion part consisted of a curve (R=3mm) to replicate the transition region from corroded to healthy. The height of the corroded part is obtained from Khurram et al., (2014) who identified that the buckling mode would appear if the corroded height was greater than 60 mm.

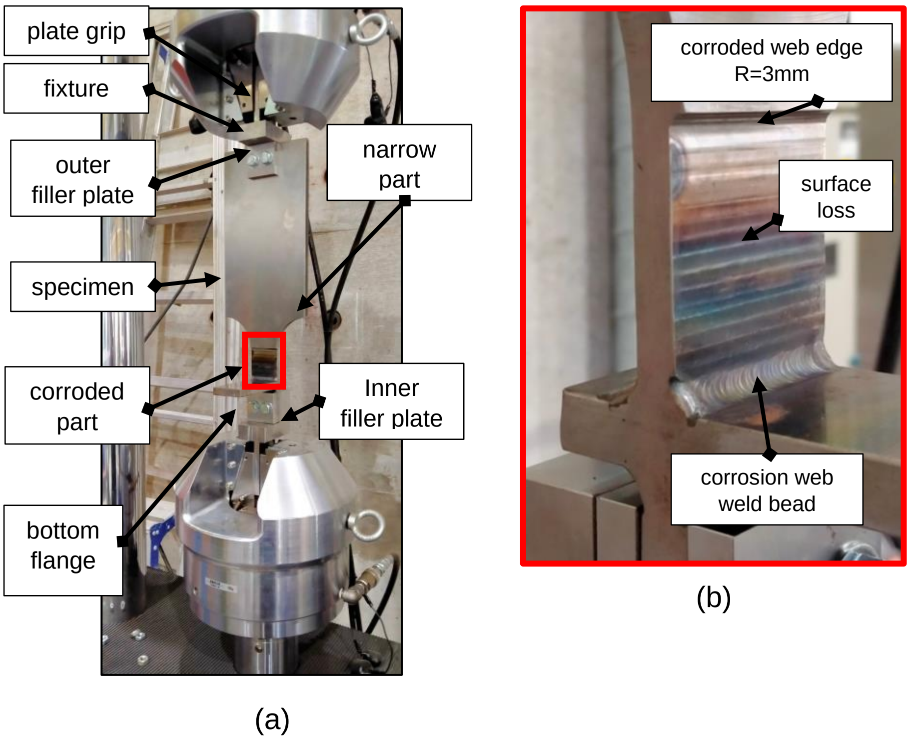

Figure 3 (a) Compact specimen setting placement before repairment; (b) Target part.

The reason why the corrosion damaged area in this specimen is uniformly thinned is that the surface irregularities caused by corrosion are assumed to have been smoothed out prior to the attachment of CFRP.

3. Experimental Setup

The experimental setup described in this study was conducted to provide adequate data for determining the dependence of CFRP durability against fatigue damage initiation (Chandran et al., 2017; Liu et al., 2017; Baumgartner et al., 2019). This can be explained based on the elastic response over the number of cycles. The method is applied to steel members under normal stress due to bending moment, and axial force (including reaction force). The method is intended to reduce the stress level and improve the load capacity of steel members with section loss by preventing buckling. CFRP reinforcement may degrade from its edge where the stress is concentrated. Thus, this study proposed a new parameter related to the practical definition of CFRP damage initiation as "the period required to produce damage into visible size."

- **Design Load**

Based on the data provided by Nippon Expressway Research Institute (NERI), the elastic modulus was evaluated for the material of each element. For Epoxy Primer (FP-N9) $E = 2533$ MPa; Epoxy Putty (FB-ES9) $E = 4021$ MPa; Polyurea Putty (FU-Z) $E = 65$ MPa; CFRP-resin (FR-E9P) $E = 640000$ MPa; Steel $E = 210000$ MPa. As shown in **Figure 4(a-c)**, the C3D8R element is applied to the remaining elements, except the CFRP part (SR4), to capture an accurate stress concentration in a dense mesh. However, the thickness of CFRP is 0.143 mm per layer. The element joint is modeled as a monolith (tie constraint) with various material properties to support a simple attachment element.

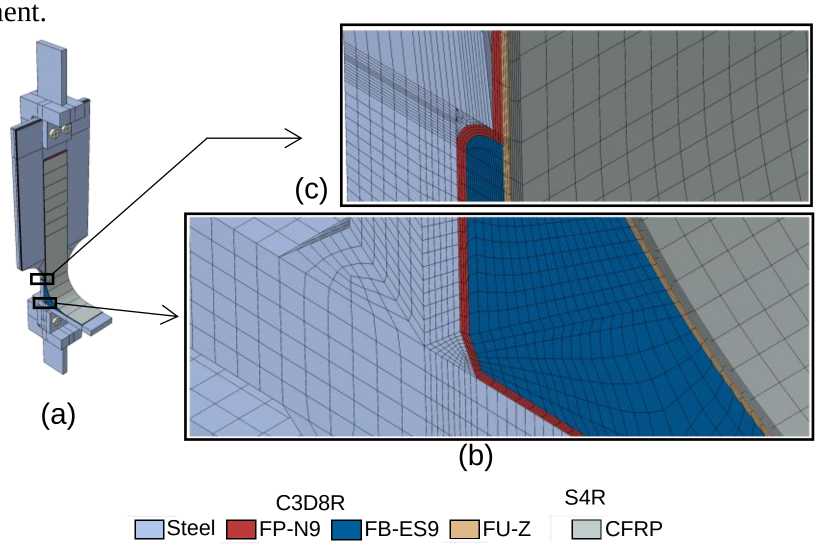

Figure 4 a) CFRP retrofit specimen model; (b) Detailed mesh of the corroded weld part; (c) Detailed mesh of the corroded web edge

The reproduction of local stress between three-dimensional models is necessary for shape-based structure verification control. A comparison of the local stress distribution describes the reproduction of the service load of the CFRP retrofit sub-model steel girder end to the CFRP retrofit specimen. The local stress distributions are determined using the trial load of the retrofit specimen and then verified to the value of local stress at the girder ends until it is agreed. The approach key is the elastic local stress distribution shown in **Figure 5(a-b)**, which should coincide with each other (retrofit sub-model and retrofit specimen) to generate typical conditions. The local stress of the steel member should be examined by measuring stress level before and after CFRP application. The local stress distributions of the selected CFRP retrofit steel girder ends with cross-beam bracing are referred to as the Noor and Tamura (2022) results. The reproduction of the service load ($LL+DL$) on the retrofitted specimen was 55 kN (P_{LL}) and the dead load was 15 kN (P_{DL}).

When determining the fiber direction of CFRP on the corroded web end plate around the vertical stiffeners, more attention should be paid to the compression zone ($12t_{web}$) of the web plate end where bending buckling occurs before shear buckling. Therefore S22 (vertical normal stress) is focused on the stress state comparison.

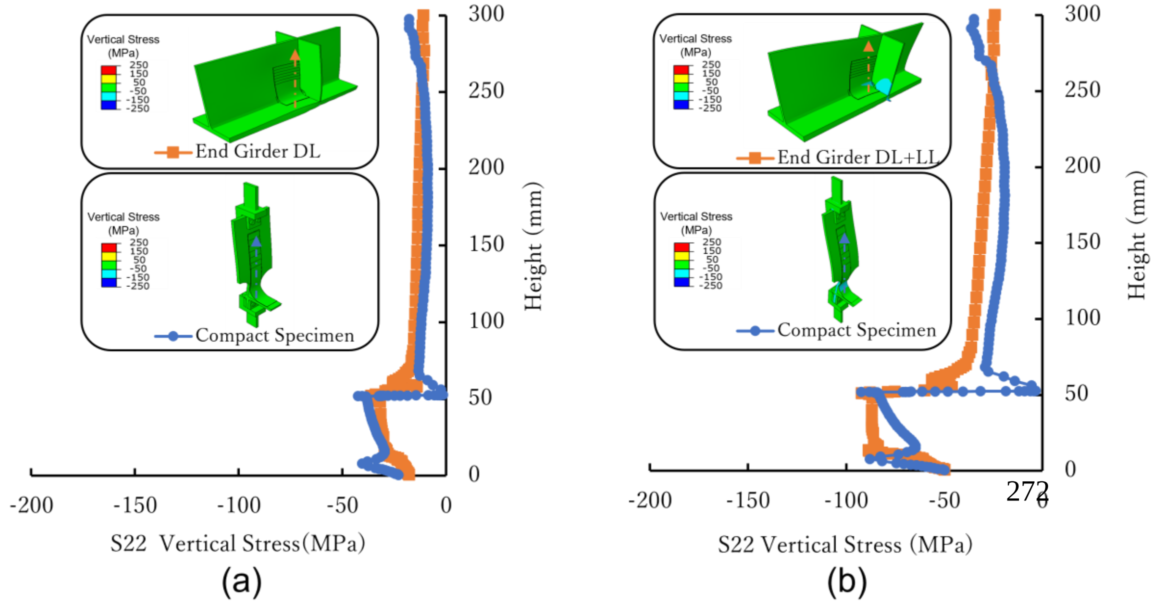

Figure 5 (a) Loading determination of dead load (15 kN); (b) Loading determination of case 2 live load + dead load (55 kN)

- **Polyurea Putty (FU-Z) Configuration**

In this section, we have discussed the importance of the usage of polyurea putty. If the utilization of polyurea putty is neglected, the CFRP will delaminate or detach because it is incapable of maintaining the out-of-plane deformation of steel (bending mode case). In one of the previous research works (Wakabayashi et al., 2012), the effect of polyurea putty (FU-Z) on the buckling deformation of CFRP-reinforced steel plates is studied. It was observed that the maximum load with polyurea putty was not significantly different from that without putty. However, the polyurea putty prevents the load from suddenly decreasing when the displacement exceeds its ultimate value. Polyurea putty in CFRP sheets could improve flexibility and prevent debonding due to buckling mode. Furthermore, Hidekuma et al., (2020) designed no-putty cases with an epoxy primer (FP-N9) and an impregnation epoxy resin (FR-E9P). It was thickened by adding 1/3 of its initial thickness to avoid a significant error in the stress concentration of the epoxy primer as the first layer. Therefore, in principle, when the temperature is lower than 5°C or the humidity is higher than 85% on rainy days, this retrofitted method should not be applied (NERI, 2015).

- **Frequency Determination**

According to Biggs et al., (1956), the vibrations of simple-span bridges with different span lengths are compared. Then, based on the field measurement, the Gilbertville Bridge (34.7 m) was purposely chosen to use its natural frequency (4 Hz) as the input parameter to the loading machine. The selected bridge is closest to the span length and type of the target bridge that has been studied by Noor and Tamura (2022).

- **Experimental Loading Strategy**

To perform a durability experiment on fatigue, uncertain parameters, such as temperature and creep should be clarified first. **Figure 6a** shows the loading strategy used to reproduce a state similar to that of the fatigue experiment. The experimental setup is placed near the testing machine, which is used in the fatigue experiment, at ambient temperature. The temperature-driven experiment aims to observe the relationship between the temperature differences in the CFRP reinforcement part. The purpose of the creep experiment was to understand the amount of strain change caused by creep deformation that occurred in each part of the retrofit component under constant load conditions. Because the durability experiment required an extended time, this parameter is clarified before the cyclic loading begins

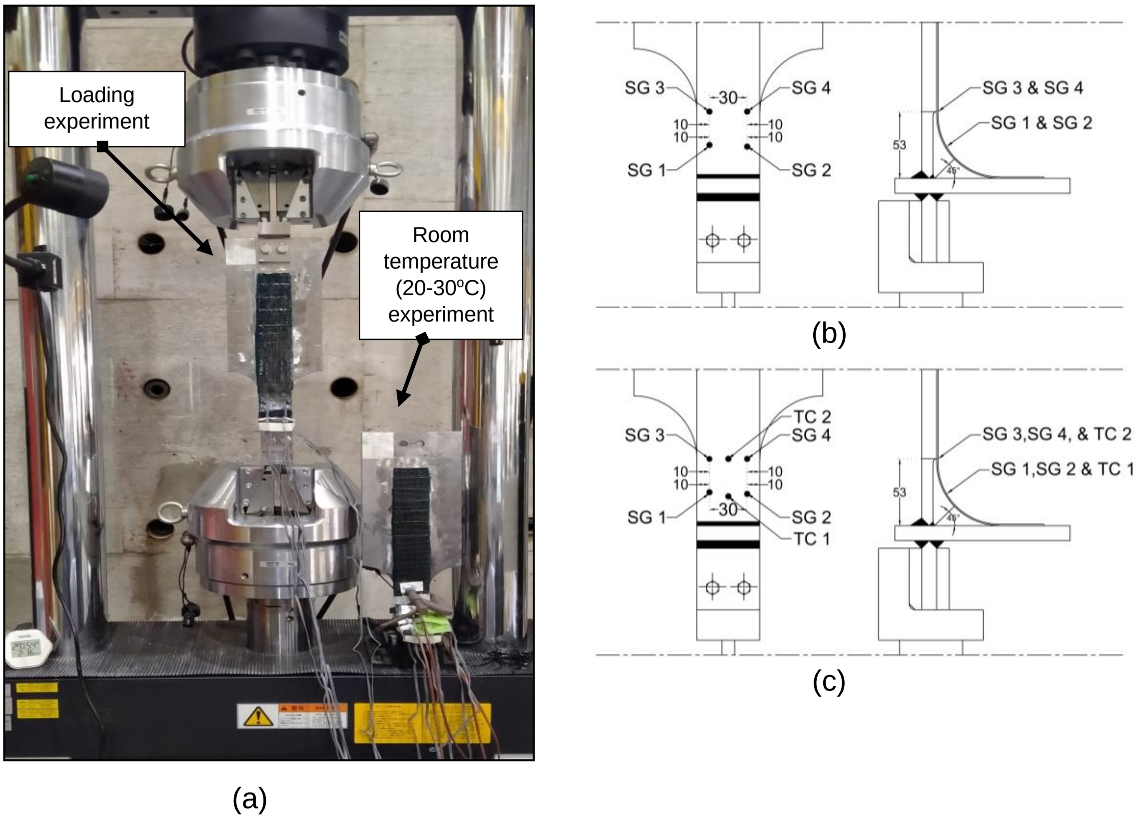

Figure 6 (a) Experimental conditions; (b) Location of strain gauge (SG) during loading experiment; (c) Location of SG and thermocouple (TC) in temperature experiment (unit: mm)

The strain gauge is attached to the CFRP surface with a similar arrangement for each retrofitted specimen as shown in **Figure 6(b-c)**. Four points of the strain gauge are placed on the CFRP surface. The strain gauge points are selected based on the numerical analysis of the specimen for high local stress locations on the CFRP. A thermocouple type T-G-0.65 from Tokyo Measuring Instruments was utilized. Moreover, the strain gauge type BFLAB-2-3-3LJCT-F for the composite material (CFRP) manufactured by Tokyo Measuring Instrument adhered to an epoxy-based long-term measurement adhesive EB-2. The strain gauges were attached at the same four locations as in the fatigue experiment (referred to as strain gauge 1) based on the numbering shown in **Figure 6(b-c)**. Two thermocouples were installed between the strain gauge attachment positions to generate local temperature changes in the CFRP components.

The experiment was performed using a fatigue machine EHF-EV200k1 (a dynamic fatigue test system manufactured by Shimadzu Corporation, Kyoto, Japan). A compressive load of 55 kN was applied as a preload to fit the jig and fixtures in the same manner as fatigue loading. Subsequently, the loading continued to maintain a compressive load of 15 kN as the minimum value (self-weight) during the fatigue experiment for three days and attached to the strain gauge. Then, the creep strain of each part was measured. The strain gauge was attached at the same position as the cyclic load and the measurement was performed at a sampling rate of 0.1 Hz. Subsequently, the local strain on the retrofitted specimen was saturated under an isotropic pressure of self-weight before applying cyclic loading. The focus of the measurements was to saturate the strain at a selected load (15 kN). The creep experiments were conducted at 20-30°C temperature. Because no creep rupture was observed under this condition, the strain-time relationships were considered in two stages, as presented in **Figure 7(a-b)**. In the first stage, the strain increases following the saturation of the fiber and resin for one day. Subsequently, the creep strain rates slow down at a constant rate and are stable for an extended period of cyclic loading. An elastic elongation mechanism is developed based on a compact specimen design under constant load to clarify the target location and deformation mode of the retrofit specimen. In **Figure 7(a-b)**, the creep strain at SG 3–4 is higher than that at SG 1–2. This indicates that the influence of the vertical force acting perpendicular to the retrofit specimen is more severe at the corroded web edge. Therefore, the local stress on the CFRP curved part should be monitored carefully because the change of fiber alignment could probably create additional stress.

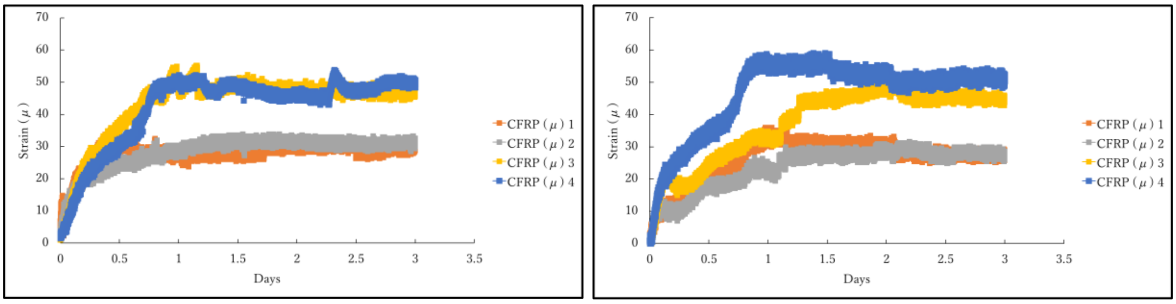

(a) (b)

Figure 7 (a) Creep strain of retrofitted specimen without putty (15 kN) (b) Creep strain of retrofitted specimen with putty (15 kN)

The initial change in the room-temperature strain was based on the CFRP resin hardening process of the retrofitted specimen without putty. The dependence of the thermoplastic behavior on the completion elastic modulus of the CFRP reinforcement is compared and plotted in **Figure 8.** The heat from the hardening process influences the increase in thermal strain for one day. Also, the linear expansion coefficient of CFRP (after the resin is impregnated with the fiber) is around 1x10^{-6}/°C, significantly smaller than that of the steel (12x10^{-6}/°C), which can be regarded as almost 0. Therefore, this behavior created adhesion at the interface of CFRP parts. It is observed that the effective temperature strain is independent of the level of elastic strain, which defines internal thermal activation. Measurements were taken every 30 s for three days during the fall season.

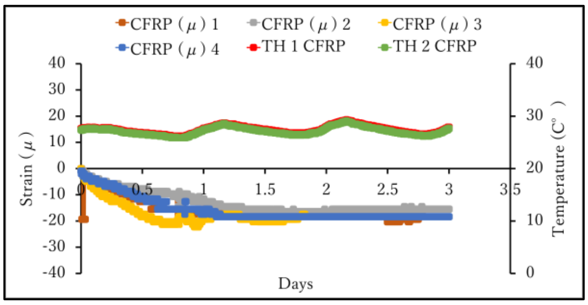

Figure 8 Characteristics of room temperature strain on CFRP part

Coupling strategies between the creep and room-temperature experiments were conducted. The relevant conditions for the loading strategies are proposed in **Figure 9**. The free-temperature thermal properties of the CFRP materials are independent. Therefore, the creep strain is induced into the cyclic loading as a reference. The experiments are performed using a previously described fatigue machine. A compression load with a sinusoidal waveform is applied at 4 Hz as seen in schematic **Figure 9**. In addition, cyclic data are collected every 10,000 cycles. To apply a cyclic load of more than one million cycles, a period of at least two days is required. The cyclic loading stopped at 3.5 million cycles that lasted for 10 days. Strain measurements were then performed intermittently such that the deformation of the retrofit specimen could be grasped in units of 10,000 cycles. The axial cyclic loading and loading-point displacements were maintained at a sampling rate of 100 Hz. The high-cycle fatigue loading continued until damage initiation appeared visually.

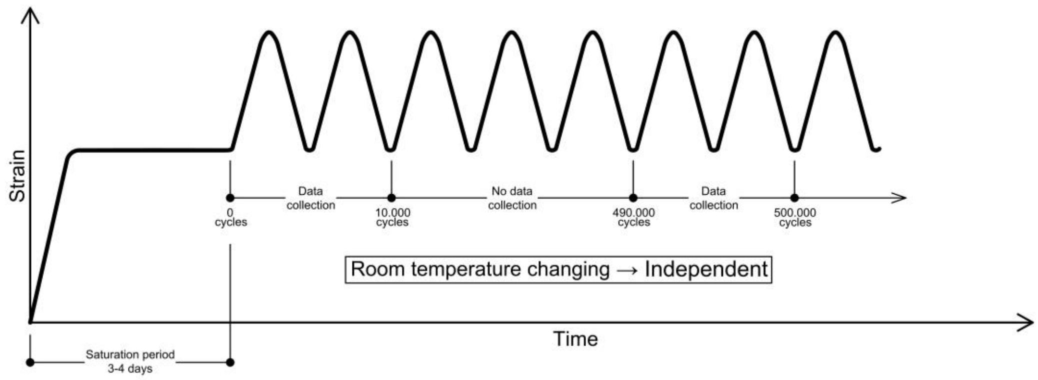

Figure 9 Schematic loading strategies of the experiment

4. Experimental Results and Observations

Detachment and delamination are the CFRP damage types that are difficult to inspect because they are concealed. Therefore, this study succeeded in using a strain gauge to detect detachment under cyclic loading and supported it with visible damage verification. Nevertheless, destructive observations have been conducted to determine the delamination characteristics of CFRP reinforcements. The CFRP-retrofitted specimens (with and without putty) were high-cycle fatigue experiments under a constant compressive load range $\Delta P = 40$ kN. The local stress at the CFRP-corroded web edge was higher because of the transition of the corroded region to the healthy region. The difference in local stress at each point was used to provide a linear response to determine the adverse region of CFRP reinforcement. Thus, the target investigation for maintaining the elastic stress of the CFRP part in the proposed method was satisfied.

- **Detachment Characterizing**

Detachment is one of the damage initiation types of CFRP-strengthened steel. At a constant load, the joint polymer particles separate owing to the direction of the mode. From the experiment specimen without putty, the detection of damage initiation is possible by using shifted local stress σ_{SLS} characteristics that indicated the change of micromechanics due to fatigue. Since the σ_{SLS} is achieved by the separation of joint bonds perpendicular to the stress direction, the elastic modulus of the CFRP maintained a constant local stress level for an extended cyclic load. In addition, the shifted local stress immediately dissipated and returned to the initiation stress level, whereas the elastic modulus of the joint material changed with time.

The detachment that occurred in the specimen without putty was achieved by the separation of joint bonds owing to the combination of the local vertical stress and the out-of-plane mode at certain cycles. The damage-initiation stress signal was detected only in SG3. Moreover, the effect of rapid deformation on the detectable detachment was visually confirmed. The comparison of durability observation in local stress measured from $2.5\text{x}10^6 – 3.5\text{x}10^6$ cycles is shown in **Figure 10**. When the joint material is suddenly deformed by the influence of a long period (3 million cycles) of eccentric cyclic loading, the shifted local stress (σ_{SLS}) of the elastic joint exhibits "impact during cyclic stress" behavior, even though the stiffness is not changed immediately or delayed as shown in **Figure 10a-2.** The sudden change in local stress detected only at the surrounding location of SG3 was observed as a stress redistribution phenomenon owing to the CFRP joint separation. The shifted local stress correlated with the release of the joint modulus. This parallel arrangement of the elastic moduli of each material is due to the constant eccentric cyclic load effect that occurs independently. After the local area of the joint material was separated, the elastic modulus immediately returned to its initial condition. Local stress redistribution of the detachment occurred in a short period, indicating that the impact stress during cyclic loading was completed. Therefore, the contribution of the high elastic modulus of CFRP (640 GPa) prevented the damaged part from losing its stiffness in the following cyclic loading. However, the detachment phenomenon must not be understood solely in terms of the geometrical findings. The cyclic load amplitude was low but sufficient to influence the CFRP reinforcement structure material. This may have resulted from the lack of flexibility in the specimen without the polyurea putty (FU-Z), which exceeded the earlier local fatigue damage. Otherwise, as shown in **Figure 10b (1-3),** the application of FU-Z stabilized the performance of the target retrofit part owing to its excellent elongation characteristics. The local stress of the putty specimen remained linear in the local stress data measured at the same cyclic level. The additional finding showed that the 1.05 mm thickness of FU-Z had a significant response to durability performance, thus supporting the CFRP strengthening method solutions.

The reversible elastic local stress in compression (C-C) fatigue loading generally shows elastic recovery for each type of detachment damage. There are four shifted local stress (σ_{SLS}) detected in 3 million cycles. This initial damage occurred between the urea primer (FP-UL1) and CFRP resin (FR-E9P). As shown in **Figure 10c** the 1st damage detection was performed for 7 s with 28 cycles (2991818 – 2991846). The one of cyclic stress was attached to the zero stress (σ_0), which means elastic modulus (E_0) was not active. A cyclic impact effect was observed where the elastic modulus consisted of the bending stress concentration. In this investigation, the characteristics of the CFRP material can be described as the control parameter after initiating local damage. This was because improving the load capacity against the eccentric cyclic compressive load was essential when the CFRP part was damaged owing to this combination. In addition, the standard value of tensile strength in the aligned fiber direction was specified as 1.900 N/mm^2 (NERI, 2015). The separation of the CFRP joint has been proven to be harmless to the CFRP part. The behavior of the CFRP material can be adapted to operating cyclic loads when experiencing the initiation of detachment. The local damage characteristics of the CFRP contributed to the corroded steel reinforcement owing to the dissipating stress concentration, and out-of-plane deformation under elastic conditions was discovered. Therefore, the putty specimen exhibits a strong material bond. In addition, as shown in **Figure 10b (1-3)**, it can be interpreted that the fatigue life improvement of the CFRP reinforcement by polyurea putty was related to the viscoelastic behavior. Using polyurea putty (FU-Z) is one of the factors that significantly improved the durability and strength of the reinforcement part.

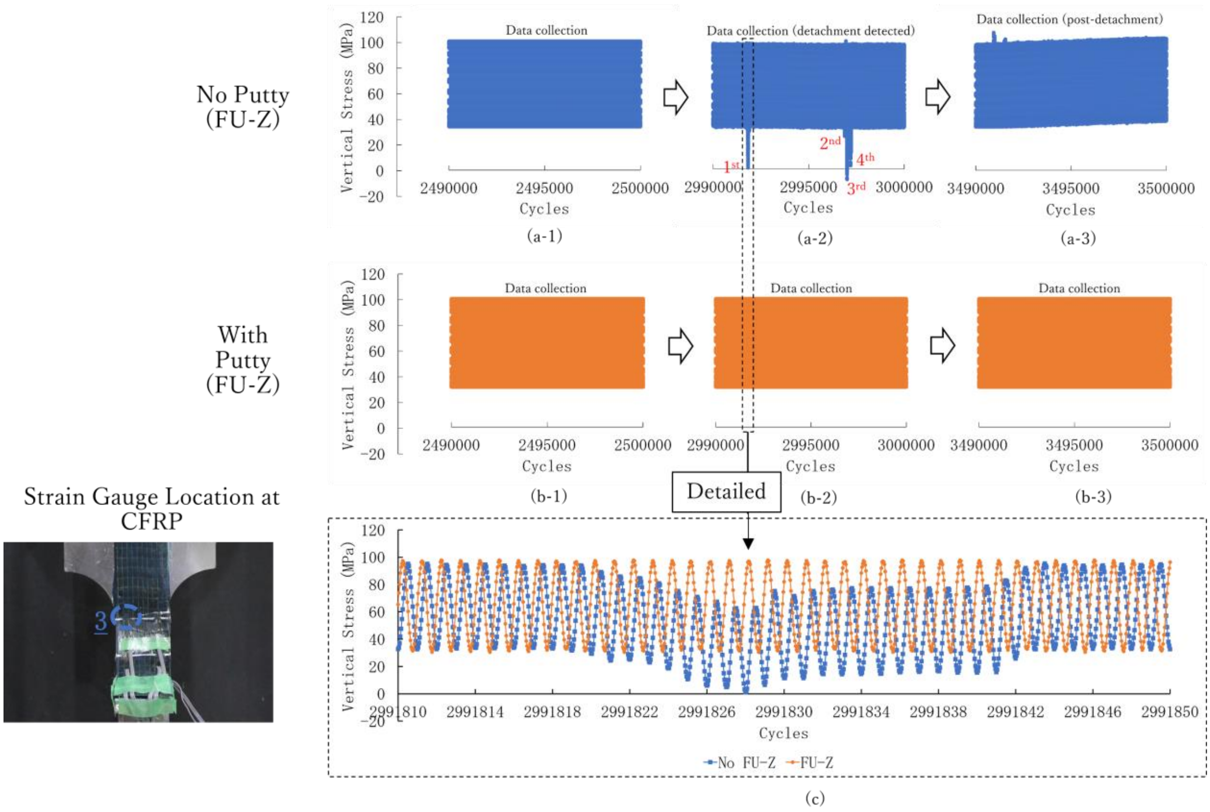

Figure 10 Data collection of local stress at 2.5-3-3.5 million cycles: (a-1) local stress data specimen without putty in 2.5x10^6 cycles; (a-2) detachment-detected data collection; (a-3) data collection of post-damage initiation in 3.5x10^6 cycles; (b 1-3) specimen with putty; and (c) detailed comparison of cyclic loading with 1st damage initiation.

The effect of cycles (N) showed that the interactions between cyclic loading and damage initiation were complex. These relationships are challenging to integrate into the service life prediction model as shown in **Figure 10a-2** for 3 million cycles. However, the 2nd damage detection signal had different characteristics. The local stress decreases by 8 MPa. The element parts still have an elastic modulus; therefore, detachment cannot occur perfectly. The 3rd damage detection was for 9 s and it reached the zero stress (σ_0), thus indicating that full detachment occurred. The 4th damage detection was 11 s long and almost reached zero stress. The difference in the local stress was approximately 2 MPa. All the detachment processes were detected for 31 s with 124 cyclic damage loads. The detachment process reveals the possibility of fully separating the joint material under rapid conditions. The strain gauge successfully captured the initiation deformation mode of the specimen without putty. The cyclic damage block was redistributed over a noticeably short period.

In the final loading of 3.5 million cycles, the detachment characteristics showed a slight inclination of the local stress. When detachment is initiated, progressive detachment is defined without an increase in the compressive fatigue load. The inclination of the local stress, as displayed in **Figure 10a-3**, results from the slight out-of-plane displacement in the detached region. The instability of the thin CFRP laminate owing to detachment was measured as a change in the local stress. The change in local stress during constant-amplitude cyclic load fluctuations plays an important role in determining the detachment effect after the initiation phase. Moreover, because the detachment slip maintains an elastic condition, the bond strength of the damaged joint transmits the residual stress to the effective bond joint area.

- **Damage Visibility (Detachment)**

A visible detachment location of the damage in the specimen without putty was identified in this study. This location represents the elastic stress concentration in the retrofit specimen. Joint urea primer and CFRP-resin separation were identified as damage-initiation characteristics. Damage initiation was detected by visual inspection as shown in **Figure 11**, only at the left-side corroded web edge within the vicinity of the growth end. Therefore, the elastic deformation in the corroded web edge is not uniform. This condition is known as the "resin-rich zones" effect (Hwang et al., 2001; Koutsonas, 2018; Haesch et al., 2015; Ahmadian et al., 2020). They are formed during the CFRP-resin construction process.

The detachment slit was measured as approximately 2.02 mm after the cyclic loading was complete. The length of the damage growth on the upper side was approximately 14 mm and that on the bottom side was approximately 16 mm, as shown in **Figure 11**. After joint separation, the damage can grow in the matrix owing to the bending mode. This was because, the high frequency of the bending mode reduced the strength of the matrix. It can be observed from **Figure 11** that, the top end of the corrosion zone should be further considered as a potential damage region at CFRP retrofit girder ends.

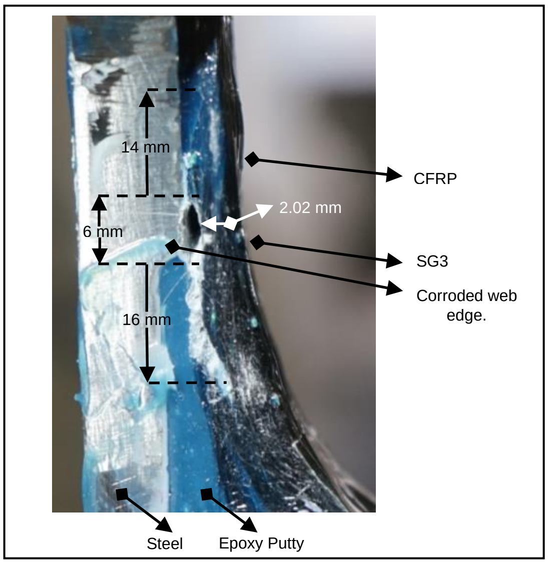

Figure 11 Damage initiation with the detachment of the interface CFRP reinforcement part in the specimen without polyurea putty (FU-Z)

- **Interlaminar Failure (Delamination)**

During the fatigue loading of the specimen without putty, a local stress (σ_{LS}) concentration in vertical direction and magnification of detachment area created fiber–resin debonding condition. The process of internal delamination began with the spread of detachment. Delamination is observed at the end of the loading cycle (3.5 million cycles). The method to check the delamination process was examined by cutting the specimen at detachment points. The micro delamination of the specimen was then captured. As shown in **Figure 12 (a-b),** a comparison of the cut sections of the specimens with and without putty is evaluated. Strain gauge location (SG3) was used to verify the strain results and visual damage. This study also verified the contribution of the corroded web edge to the corroded part. As shown in **Figure 12a**, delamination is observed in the outermost layers (7 → 4 CFRP sheets). The delamination gaps are measured from the cut section of SG3 at 500x magnification. The gap widths are measured from 0.3 – 0.35 mm, respectively. The typical delamination in the bridging zone length under a cyclic load was also investigated. This characteristic is recognized as the viscoelastic deformation of the tip zone during each load cycle where the compressive cyclic load denotes the traction stress at the beginning of the detachment to generate debonding. In addition, there is sufficient evidence in this study on the delamination damage in specimens without FU-Z after the detachment strike. The specimen with FU-Z was safe from delamination as shown in **Figure 12b.** The putty material prevented internal delamination in the CFRP reinforcement structure.

The proposed study contributes to a better understanding of internal delamination at the corroded web edge of the corrosion region. Delamination is primarily caused by stiffness degradation after joint separation (detachment). The bending of the local stress flowed through all the layers and caused damage in 50% of the layers as shown in **Figure 12a.** It can be seen in this experiment that the putty can prevent the internal damage that occurs in the CFRP and can avoid a situation in which a state of fatigue can occur.

Delamination may develop inside the CFRP component without being noticed on the surface. Subsequently, the adhesion between the CFRP sheet layer and resin (FR-E9P) caused the separation. This was because of the low elastic modulus of the resin bound to the CFRP sheet. The matrix was the weakest part of the CFRP laminate. However, the specimen without FU-Z survived until 3x10^{6} cycles, indicating that the material of the strengthened steel girder ends reached the design fatigue life (2x10^{6} cycles).

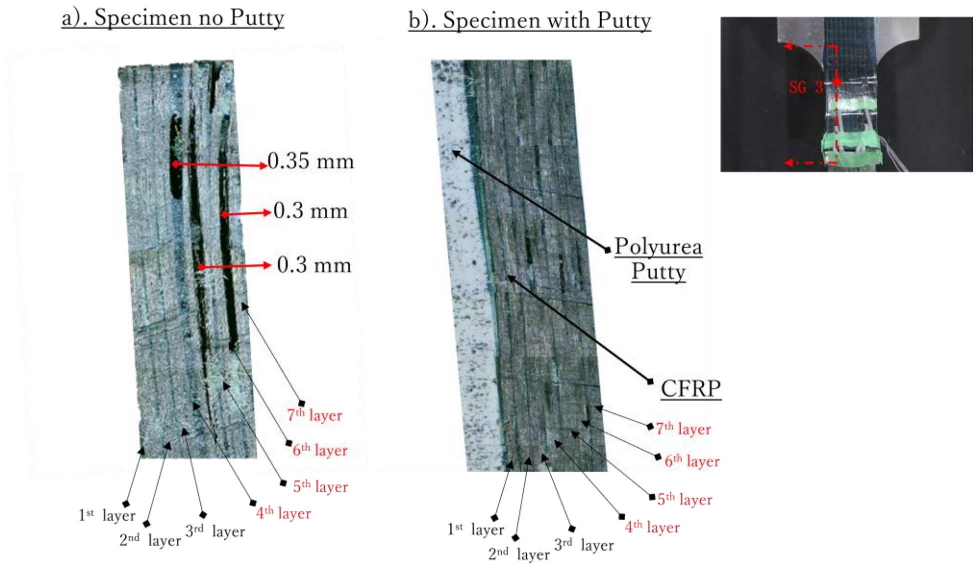

Figure 12 Comparison of damage at SG3

Furthermore, the polyurea putty (FU-Z) would like to be unable to perform at its proper capacity when the temperature is below the glass transition temperature. It will end up losing its rubber-like elasticity and becoming brittle. Therefore, the upper limit of glass transition temperature is set to maintain the required elasticity even under cold winter environments.

5. Conclusions

In this study, we assessed the durability performance of CFRP retrofit steel girder ends against fatigue using a new compact specimen model. The compact specimen with the CFRP retrofit showed cycle fatigue endurance when constructed according to the guidelines and specifications. Finally, the essential characteristics related to the CFRP-strengthened material of the specimens were investigated. Detachment and delamination were confirmed as the parameters responsible for the damage initiation. The following findings were obtained from this study:

1. This study proposed a novel experimental model for the eccentric loading mode reproduction of a CFRP retrofit steel girder end to determine the characteristic damage initiation. The element part configuration of the assessment consisted of a corroded specimen with a narrowing part, a bending fixture, and a filler plate. The advantages of the new model were simplicity of construction, maintenance of elastic fatigue, buckling resistance during cyclic compression, and effectiveness in obtaining fatigue characteristics. The proposed method provided a general method for determining the service live load control for a CFRP retrofitted steel girder end-durability evaluation. The cyclic loading value was determined using a local distribution reproduction method. Subsequently, the local stress and deformation of the CFRP retrofit specimens were localized to resemble the location of the CFRP retrofit girder ends.

2. The physical response of the CFRP reinforcement at the corroded steel girder end specimen under service loads was also observed. It should be noted that the CFRP retrofitted specimens affected all local damage responses without polyurea putty (FU-Z). Linear elasticity was identified as the most significant of these characteristics because it described the initial response of the specimen to constant amplitude load fluctuations, whereby the CFRP damage part was able to return to its original state after damage initiation. Whenever purely elastic deformation occurred at the CFRP part, it could be recognized as an "impact stress"; however, the elastic modulus changed independently with 5×10^5 cycles. This behavior was observed when the shifted local stress during the deformation stages did not exceed the elastic limit. In this process, the interlaminar stress of the CFRP joint led to redistribution for the instance cyclic period. Furthermore, some deformations were visible and permanent. However, owing to the high elastic modulus of CFRP, it can endure large amounts of cyclic loading so that the corroded steel girder is safe.

3. Two initial damage characteristics were observed in the CFRP retrofitted specimen without FU-Z under cyclic loading: detachment and delamination. The initial macroscopic damage was located at the end of the corroded web edge. Because the elastic modulus of each element was typically stronger than that of the joint itself, detachment occurred in the joints earlier than the delamination of the CFRP layers. It took $3x10^6$ cycles to detect detachment so that the shifted local stress (σ_{SLS}) was announced as measured to monitor the detachment of joints. During eccentric constant compression cyclic loading, the detached CFRP could not resist its bonding interface (CFRP fiber resin (FR-E9P)). Delamination within the CFRP occurred at the same location after detachment. The specimens in this study were developed to verify the fatigue durability of CFRP attached to steel girder ends, focusing on the high stress region around the vertical stiffeners. The observed damage was not observed in the center of the specimen, which reproduces the high stress region, but near the ends. Although the boundary conditions at the ends were different from those of the CFRP on steel girder ends, the center of the specimen was shown to have higher fatigue durability than ends of specimen shown the detachment and delamination. Hence, understanding the impact of damage initiation will help engineers to estimate the fatigue durability of CFRP reinforcements at corroded steel girder ends over service life periods.

References

[1] Japan Public Works Research Institute. 2010. *Research on Corrosion Countermeasures at Steel Bridge Girder End*. ISSN 0386-5878. (In Japanese)

[2] Shenoy, M., Zhang, J., & McDowell, D. L. (2007). Estimating fatigue sensitivity to polycrystalline Ni-base superalloy microstructures using a computational approach. *Fatigue Fracture Engineering Material Structure*, 30(10), 889–904. https://doi.org/10.1111/j.1460-2695.2007.01159.x

[3] Colombi, P. & Fava, G. (2012). Fatigue behavior of tensile steel/CFRP joints. *Composite Structures*, 94(8), 2407–2417. https://doi.org/10.1016/j.compstruct.2012.03.001

[4] Yu, Q. Q., Chen, T., Gu, X. L., Zhao, X. L., & Xiao, Z. G. (2015). Boundary element analysis of fatigue crack growth for CFRP-strengthened steel plates with longitudinal weld attachments. *Journal of Composites for Construction*, 19(2), 04014044. https: //doi.org/10.1061 /(ASCE)CC .1943-5614.0000505

[5] Liu, H., Zhao, X. L., & Al-Mahaidi, R. (2009). Boundary element analysis of CFRP reinforced steel plates. Composite Structures, 91(1), 74-83.https://doi.org/10.1016 /j.compstruct.2009.04 .032

[6] Zhang, D., Huang, W., Zhang, J., Jin, W., & Dong, Y. (2021). Prediction of fatigue damage in ribbed steel bars under cyclic loading with a magneto-mechanical coupling model. *Journal of Magnetism and Magnetic Materials*, 530,167943. https://doi.org/10.1016/j.jmmm.2021.167943

[7] Wakabayashi, D., Miyashita, T., Okuyama, Y., Kobayashi, A., Hidekuma, Y., Horimoto, W., & Nagai, M. (2013). Repair method using CFRP for corroded steel girder ends. *In Fourth Asia-Pacific Conference on FRP in Structures* (pp. 1-6).

[8] Ghahremani, K., Walbridge, S., & Topper, T. (2015). Inhibiting distortion-induced fatigue damage in steel girders by using FRP angles. *Journal of Bridge Engineering*, 20(6), 04014085. https://doi.org/10.1061/(ASCE)BE.1943-5592.0000678

[9] Al-Salih, H., Bennett, C., & Matamoros, A. (2021). Evaluation of novel combined CFRP-steel retrofit for repairing distortion-induced fatigue. *Journal of Constructional Steel Research*, *182*, 106642. https://doi.org/10.1016/j.jcsr.2021.106642

[10] Magi, F., Di Maio, D., & Sever, I. (2016). Damage initiation and structural degradation through resonance vibration: Application to composite laminates in fatigue. *Composites Science and Technology*, 132, 47-56. https://doi.org/10.1016/j.compscitech.2016.06.013

[11] Marco, M., Giner, E., Miguelez, M. H., & Gonzalez, D. (2021). On the effect of geometrical fiber arrangement on damage initiation in CFRPs under transverse tension and compression. *Composite Structures*, 274, 114360. https://doi.org/10.1016/j.compstruct.2021.114360

[12] Skinner, T., Datta, S., Chattopadhyay, A., & Hall, A. (2019). Fatigue damage behavior in carbon fiber polymer composites under biaxial loading. *Composites Part B: Engineering*, 174, 106942. https://doi.org/10.1016/j.compositesb.2019.106942

[13] Ammar, M. M., Shirinzadeh, B., Zhao, P., & Shi, Y. (2021). An approach for damage initiation and propagation in metal and carbon fiber hybrid composites manufactured by robotic fiber placement. *Composite Structures*, 268, 113976. https://doi.org/10.1016/j.compstruct.2021. 113976

[14] Noor, R., & Tamura, H. (2022). Numerical Assessment of CFRP Retrofit Effect for Repairing Corroded Steel Girder Ends by Local Stress and Displacement Distribution. *Journal of Steel Structures & Construction*, *8*(7), 1-11. https://doi.org/10.37421/2472-0437.2022.08.123

[15] Systemes, D. (2018). ABAQUS Version 2018 User's Manual. Dassault Systemes Simulia Corp, Johnston, Rhode Island. https://www.3ds.com/products-services/simulia/products/abaqus/

[16] Japan Road Association. (JRA) (2012). Specification for Highway Bridge (Part II Steel Bridges). ISBN978-4-88950-717-1 C2051

[17] Nippon Expressway Research Institute (NERI). 2015. Design And Installation Manual For Upgrading of Steel Structure with The Use of Carbon Fiber Sheet. Tokyo

[18] Pham, N. V., Miyashita, T., Ohgaki, K., Hidekuma, Y., & Harada, T. (2021). Repair Method and Finite Element Analysis for Corroded Gusset Plate Connections Bonded to CFRP Sheets. *Journal of Structural Engineering*, 147(1), 04020310. https://doi.org/10.1061/(ASCE)ST.1943-541X. 0002862

[19] Baumann, A., & Hausmann, J. (2021). Compression fatigue testing setups for composites—a review. *Advanced Engineering Materials*, 23(2), 2000646. https://doi.org/10.1002/adem.20200 0646

[20] Chandran, S., Verleysen, P., Lian, J., Liu, W., & Münstermann, S. (2017). Design of an experimental program to assess the dynamic fracture properties of a dual-phase automotive steel. *Procedia engineering*, 197, 204-213. https://doi.org/10.1016/j.proeng.2017.08.097

[21] Liu, Z., Guo, T., Huang, L., & Pan, Z. (2017). Fatigue life evaluation on short suspenders of long-span suspension bridge with central clamps. *Journal of Bridge Engineering*, 22(10), 04017074. https://doi.org/10.1061/(ASCE)BE.1943-5592.0001097

[22] Baumgartner, J., Yıldırım, H. C., & Barsoum, Z. (2019). Fatigue strength assessment of TIG-dressed welded steel joints by local approaches. *International Journal of Fatigue*, 126, 72-78. https://doi.org/10.1016/j.ijfatigue.2019.04.038

[23] Gil-Martín, L. M., Šćepanović, B., Hernández-Montes, E., Aschheim, M. A., & Lučić, D. (2010). Eccentrically patch-loaded steel I-girders: The influence of patch load length on the ultimate strength. *Journal of Constructional Steel Research*, 66(5), 716-722. https://doi.org/10.1016/j.jcsr.2009.12.012

[24] Graciano, C., & Uribe-Henao, A. F. (2014). Strength of steel I-girders subjected to eccentric patch loading. Engineering structures, 79, 401-406. https://doi.org/10.1016/j.engstruct. 2014.08.031

[25] Khurram, N., Sasaki, E., Kihira, H., Katsuchi, H., & Yamada, H. (2014). Analytical demonstrations to assess residual bearing capacities of steel plate girder ends with stiffeners damaged by corrosion. *Structure and Infrastructure Engineering*, 10(1), 69–79. https://doi.org/10.1080/15732479.2012.697904

[26] Hidekuma, Y., & Ishikawa, T. (2020). Strengthening Effect of CFRP Bonded Steel Plate with Insufficient Bond Length. 5th International Conference on Smart Monitoring, Assessment and Rehabilitation of Civil Structures, August 2019 in Potsdam, Germany. e-Journal of Nondestructive Testing. Vol. 25(1). https://www.ndt.net/?id=24988

[27] Biggs, John M., and Herbert S. Suer. "Vibration measurements on simple-span bridges." Highway Research Board Bulletin 124 (1956) Pages 1-15.

[28] Hwang, S. F., & Mao, C. P. (2001). Failure of delaminated interply hybrid composite plates under compression. *Composites Science and Technology*, 61(11), 1513-1527. https://doi.org/10.1016/S0266-3538(01)00048-3

[29] Koutsonas, S. (2018). Modelling race-tracking variability of resin rich zones on 90 composite 2.2 twill fibre curved plate. *Composites Science and Technology*, 168, 448-459. https://doi.org/10.1016/j.compscitech.2018.08.001

[30] Haesch, A., Clarkson, T., Ivens, J., Lomov, S. V., Verpoest, I., & Gorbatikh, L. (2015). Localization of carbon nanotubes in resin rich zones of a woven composite linked to the dispersion state. *Nanocomposites*, 1(4), 204-213. https://doi.org/10.1080/ 20550324.2015.1117306

[31] Ahmadian, H., Yang, M., & Soghrati, S. (2020). Effect of resin-rich zones on the failure response of carbon fiber reinforced polymers. *International Journal of Solids and Structures*, 188, 74-87. https://doi.org/10.1016/j.ijsolstr.2019.10.004